

# TRANSMISSION COEFFICIENT OF TOLLMIEN-SCHLICHTING WAVES UNDERGOING SMALL INDENTATION/HUMP DISTORTION

Hui Xu<sup>\*,\*\*</sup>, Spencer Sherwin<sup>\*</sup>, Philip Hall<sup>\*\*</sup>

<sup>\*</sup>Department of Aeronautics, Imperial College London, 180 Queen's Gate, London, UK

<sup>\*\*</sup>Department of Mathematics, Imperial College London, 180 Queen's Gate, London, UK

**Keywords:** Tollmien-Schlichting wave, transmission coefficient, boundary layer instability, transition to turbulence

## Abstract

Behaviours of Tollmien-Schlichting (T-S) waves experiencing small localized imperfection distortions within the boundary layer along a flat plate are investigated. According to the theoretical results [1], for hump and indentation distortions, transmission of T-S waves shows that  $+h$  (hump) can stabilize T-S waves and  $-h$  (indentation) can destabilize T-S waves. Here, we consider the properties of the boundary layer distorted by small-scale localized imperfection with the width scale  $d$  which is less than T-S wavelength  $\lambda_{TS}$ . We analysis the shear stress distribution on the wall from both a theoretical and a numerical point of view. Then, the transmission behaviours of T-S waves are investigated numerically. We observe that for  $h \lesssim \mathcal{O}(xRe^{-5/8})$ , both hump and indentation have destabilizing effects. By observing the profiles of the T-S wave transmission coefficient distributions around short rapid distortions, we observe that recovering the Blasius boundary layer profile is only required after a long distance from the rapid distortion position and the distance is far greater than  $\mathcal{O}(xRe^{-3/8})$ , since the shear stress distribution has a profound influence on both upstream and downstream of the rapid distortion position. Therefore, there is no Blasius boundary layer velocity profiles on the scale  $\mathcal{O}(xRe^{-3/8})$ , then, estimating theoretically T-S wave transmission coefficient for the current configuration  $h \lesssim \mathcal{O}(xRe^{-5/8})$  is inapplicable. Therefore, the classical linearised triple-deck

theory can not be employed to formulate a universal analytical expression of the transmission coefficient. Finally, it is concluded that the mechanism of the T-S wave destabilization is shown to be independent of roughness types.

## 1 Introduction

In the boundary layer located along the wall as flow moves downstream, laminar-turbulent transition is often triggered by growth of small amplitude perturbations and subsequent breakdown of perturbations. The Tollmien-Schlichting (T-S) wave is such a perturbation. In a low-level disturbance environment such as free flight, the process of laminar-turbulent transition is subdivided into three stages: receptivity, linear eigenmode growth and nonlinear breakdown to turbulence. The instability of T-S waves is the second stage of this process, the mathematics for which was established nearly 80 years ago [2]. T-S instability waves grow in accordance with linear stability theory until nonlinear and three-dimensional effects contribute to the flow breakdown to turbulence. Since the existence of T-S instability was confirmed [3], there have been many studies undertaken to explore and further explain transition.

T-S waves are eigenfunctions of the Orr-Sommerfeld equation, which is a fourth-order linear ordinary differential equation derived from the linearised Navier-Stokes equations based on the assumption of parallel flows [2, 4]. Solutions of the Orr-Sommerfeld equation are used to de-

scribe the stability property of parallel base flows. In order to predict transition to turbulence, the amplification factors of T-S waves along streamwise direction are estimated. Practically, the estimation of amplification factor is independent of free-stream disturbances' environments and tiny localized imperfection on the wall (or local curvature variation of the wall). Free-stream disturbances are related to the receptivity mechanism, which have been widely discussed from experimental, theoretical and numerical aspects [5, 6, 7, 8, 9, 10]. Addressing the interaction between T-S waves and *rapid distortion* on the wall has practical significance for prediction of laminar-turbulent transition [10].

For small-amplitude roughness which is located in the viscous sub-layer and has a slight modification of the streamwise component of the boundary layer base flow profile, such modification on transition has not been fully understood. From both theoretical and numerical points of view, only the receptivity mechanism of isolated roughness with small height is well understood [11]. The receptivity mechanism indicates that any departure from surface smoothness can excite T-S waves by interacting with free-stream disturbances or acoustic noise. For distributed roughness, it is inferred that the faster growth of T-S waves on the rough wall was not attributed to a destabilization effect of roughness such as inflectional instability behind an isolated roughness and claimed that the growth is due to the continual excitation of T-S waves on rough wall by free-stream turbulence [13]. The problem of the effect of distributed roughness on the stability and transition still remains open. Thanks to uncertainty of experiments, the reason is difficult to be derived for either isolated roughness or distributed roughness. By virtue of numerical simulations, it is discovered that the influence of two-dimensional humps and steps on the stability characteristics of a two-dimensional laminar boundary layer by the direct numerical simulation (DNS) based on the vorticity-velocity formulation of the complete Navier-Stokes equations (NSEs) for incompressible fluids and showed that a localized rectangle hump destabilizes the laminar boundary layer

[14]. Recently, it is found that this conclusion is inconsistent with the asymptotic theoretical prediction [1]. Fundamentally, a full understanding about isolated/distributed roughness on the stability property of the laminar boundary layer has particular theoretical and practical significances for understanding the laminar-turbulent transition in the boundary layer.

In this paper, our interest is to study behaviours of T-S waves numerically when base flows are distorted by rapid varying localized imperfection on the wall and understand whether or T-S waves are energized or weakened. The description of the interaction between T-S waves and localized imperfection depends on the generation of base flows. Profiles of base flows around small localized roughness change rapidly for subsonic flows, the theoretical description of which is generally given by the triple-deck theory. However, the practical limitation on triple-deck solutions is their extended downstream-wake behavior at  $X \gg 1$  as governed by the slow algebraic-fractional power-law decay in the interactive pressure and skin-friction disturbances [15]. The power-law decay conditions were only obtained by manipulating linearised lower-deck solutions. Moreover, at  $X \geq 2$ , the parallel shear-flow assumption is questionable underlying the triple-deck theory. In reality, the streamwise development of base flows becomes influential. Numerical investigation in the paper shows that when  $X > 30$ , for flat plate cases, the approximate Blasius flow profiles could recover. Supposed that the triple-deck model is solved numerically, in order to generate acceptable and available results for engineering applications, a non-linear triple-deck model must be solved and large upstream and downstream distance also must be adopted. Due to requirements of domain size, the computational complexity and cost are comparable to DNS. Besides the generation of base flows, the prediction of T-S waves around roughness is also problematic. The numerical evidence indicates based on the triple-deck theory, the localized asymptotic analysis may not produce the true behaviours of T-S waves when base flows are distorted by rapid varying localized imperfection on the wall.

Thanks to the inevitable modelling deviation from the real physics, which is generally induced by numerical strategies, the high precision numerical methodology has to be used to address the physical phenomena and handle parametric responses for the boundary layer problem. Therefore, in this paper, the spectral element method (SEM) is used to establish the discretization of the governing equations (see [16] for more details). High order curved elements are used to approach smooth roughness elements. The polynomial basis functions with eight modes are adopted to establish the discrete spectral element space to approach the variables in the governing equations. With the aid of SEM, base flows are generated by DNS of the fully non-linear Navier-Stokes equations (NSEs) with very low dissipation. T-S waves are simulated by the linearised Navier-Stokes equations (LNSEs). For base flow generation, the inlet and outlet positions are far from localized roughness locations in order to guarantee that base flows recover the Blasius profiles. In simulations of LNSEs, the most unstable Orr-Sommerfeld (O-S) eigenfunctions are prescribed as the boundary condition profiles at the inlet of the computational domain. At the outlet, sponge regions are used to damp out T-S waves.

In next section we give an introduction of the fundamental definitions related to the studied problem which we are interested in. The corresponding partial differential equations will be given. Then, the basic numerical strategies and configurations are provided in §3. The various numerical results and the discussion are given in §4. Finally, the further discussion is given and some conclusions are derived for the distortion of both humps and indentations.

## 2 Preliminaries

The non-dimensional momentum and continuity equations for an unsteady viscous fluid with constant density are defined by

$$\begin{cases} \partial_t u + u \cdot \nabla u = -\nabla p + Re^{-1} \nabla^2 u \\ \nabla \cdot u = 0, \end{cases} \quad (1)$$

where  $u = (u, v, w)$  denotes the velocity,  $p$  is the kinematic pressure and  $Re$  is a Reynolds number based on streamwise distance  $L$ . For a flat plate, it is assumed that  $Re$  is large, the base flow field can be approximated by the well-known Blasius equation

$$f'''(\eta) + \frac{1}{2}f(\eta)f''(\eta) = 0, \quad (2)$$

with the following boundary conditions

$$f(\eta) = f'(\eta) = 0 \quad \text{at} \quad \eta = 0, \quad (3a)$$

$$f' = 1 \quad \text{at} \quad \eta \rightarrow \infty, \quad (3b)$$

where the prime denotes the derivative with respect to  $\eta$ . The dimensionless variables are defined by

$$f = \Psi / \sqrt{\nu U_\infty x} \quad \text{and} \quad \eta = y \sqrt{U_\infty \nu / x},$$

where  $\Psi$  denotes the stream function. Hereby, the streamwise and vertical velocity profiles of the Blasius boundary layer are calculated by

$$U_B = \frac{\partial \Psi}{\partial y} = U_\infty f'(\eta) \quad (4)$$

and

$$V_B = -\frac{\partial \Psi}{\partial x} = \frac{1}{2} \sqrt{\frac{\nu U_\infty}{x}} (\eta f'(\eta) - f(\eta)). \quad (5)$$

Further, let's consider the following linearised system for addressing behaviours of T-S waves when base flows are distorted by humps/indentations

$$\begin{cases} \partial_t \tilde{u} + \bar{u} \cdot \nabla \tilde{u} + \tilde{u} \cdot \nabla \bar{u} = -\nabla \tilde{p} + Re^{-1} \nabla^2 \tilde{u} \\ \nabla \cdot \tilde{u} = 0, \end{cases} \quad (6)$$

where  $\tilde{u}$  and  $\bar{u}$  denote the perturbed velocity vector and the base flow velocity vector, respectively. And  $\tilde{p}$  is the perturbed pressure.

Following the scales used in the triple-deck theory, we introduce the scales  $xRe^{-3/8}$  and  $xRe^{-5/8}$ , then, the following dimensional scales are defined around roughness elements

$$X = (x - x_c) / (x_c Re^{-3/8}), Y = y / (x_c Re^{-5/8}), \quad (7)$$

where  $x_c$  is the center position of roughness elements.

It is known that 2D T-S waves can be described by the following expression

$$\tilde{u}(X, Y, t) = \tilde{u}(Y) \exp(i(\alpha X - \omega t)). \quad (8)$$

For an unstable frequency  $\omega \in \mathbb{R}^+$ , the T-S wave envelope is defined by the absolute maximum amplitude of the T-S wave for all  $t \in \mathbb{R}^+$  as follows

$$A^{\max}(X) = \max \left\{ \left| \tilde{u}(Y) \exp^{-\Im(\alpha)X} \right| : \forall Y \in [0, \infty) \right\}. \quad (9)$$

With the similar definition, the distorted T-S wave envelopes for humps/indentations are denoted by the following notations, respectively

$$A_h^{\max}(X) \quad \text{and} \quad A_i^{\max}(X). \quad (10)$$

For a flat plate boundary layer, let  $A_f^{\max}(x)$  denote the absolute maximum amplitude of the T-S wave. In order to quantify the difference between  $A_f^{\max}(x)$  and  $A_{h,i}^{\max}(X)$  ( $A_{h,i}^{\max}(X)$  denotes  $A_h^{\max}(X)$  and/or  $A_i^{\max}(X)$ ), the following quantity is defined

$$\mathcal{T}_{h,i}(X) = A_{h,i}^{\max}(X) / A_f^{\max}(X). \quad (11)$$

In terms of asymptotic theory, when the Blasius boundary layer recovers for  $X \gg 1$ ,  $\mathcal{T}_{h,i}(X)$  is constant, then value of which is the so-called *transmission coefficient*  $\mathcal{T}_{h,i}(\infty)$ . Further, to investigate  $\hat{h}$ -dependence of  $\mathcal{T}_{h,i}(X)$ , we introduce another quantity  $\mathcal{T}_{h,i}^*(x)$

$$\mathcal{T}_{h,i}^*(x) = \mathcal{T}_{h,i}(x) - 1. \quad (12)$$

Similarly, we introduce the following normal direction shear stress notations

$$\tau_f(X), \tau_h(X), \tau_i(X). \quad (13)$$

Correspondingly, the following ratios are defined

$$\tau_h(X) / \tau_f(X), \tau_i(X) / \tau_f(X). \quad (14)$$

Also, the following quantities are introduced to determine  $\hat{h}$ -dependence of (14)

$$\tau_h^*(X) = \frac{\tau_h(X)}{\tau_f(X)} - 1, \tau_i^*(X) = \frac{\tau_i(X)}{\tau_f(X)} - 1. \quad (15)$$

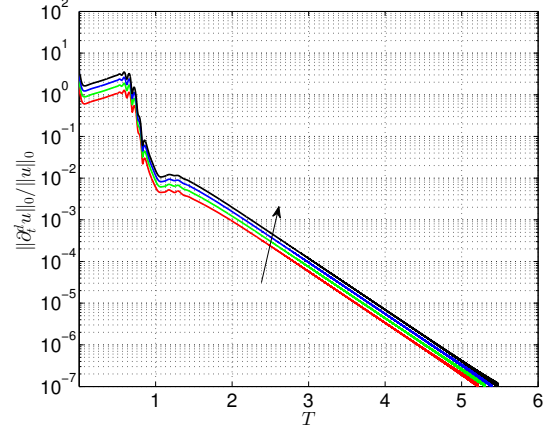


**Fig. 1** Convergent criteria  $\|\partial_t^d u\|_0 / \|u\|_0$  evolutions for the generation of base flows distorted by humps.  $Re_{\delta_*} = 1140.1$ . Height/depth  $\hat{h} = 0.6, 0.8, 1, 1.2$  and width  $\hat{d} = 1$ . The arrow indicates  $\hat{h}$  growing direction.  $T$  is a non-dimensional quantity which is defined  $t/T_c$  ( $T_c$  is a streamwise typical time scale).

In the calculations, the width ( $d$ ) and height ( $+h$ )/depth ( $-h$ ) of hump/indentation are defined according to the following relations

$$d \sim \mathcal{O}(x_c Re^{-3/8}), h \lesssim \mathcal{O}(x_c Re^{-5/8}), \quad (16)$$

and  $\hat{d} = d / (x_c Re^{-3/8})$  and  $\hat{h} = h / (x_c Re^{-5/8})$ .

### 3 Direct numerical simulations

#### 3.1 Base flows and physical configuration

We consider the boundary layer with small localized imperfection over a flat plate and define local Reynolds number,  $Re = (U_\infty \delta_*) / \nu$ , in terms of the free-stream velocity  $U_\infty$  and the local Blasius boundary layer displacement thickness at  $x_c$ . The initial conditions for solving NSEs are set by Blasius profiles. In order to guarantee steady states of (1) are obtained, a typical convergent tolerance is used as follows

$$\left\| \partial_t^d u \right\|_0 / \|u\|_0 < 10^{-7}, \quad (17)$$

where  $\|\cdot\|_0$  means the standard  $L^2$  norm and  $\partial_t^d$  denotes the discrete temporal derivative. Figure 1 illustrated the evolutions of the convergent criteria (17) for the generation of base flows distorted by humps.

With the help of DNS, we are interested in exploring behaviours of transmitted T-S waves.

Therefore, we need to study the local characteristics of base flows around localized imperfection which is located in the unstable regime according to the neutral stability diagram of the flat plate boundary layer. Numerically, to obtain high precision base flows, the body-fitted high order elements are adopted to generate mesh around roughness elements. In the computations of base flows, we set the inlet and outlet positions far from roughness position ( $X < -45$  and  $X > 45$  for upstream and downstream, respectively). Along the normal direction, the Blasius similarity variable  $\eta = y/\delta \in [0, 70]$ , the maximum value of which is used as a reference normal direction distance at localized roughness position, where  $\delta$  is the boundary layer thickness scale. By the above configuration, the obtained base flows are independent of computational domain size. The shape  $y = f(x - x_c)$  of roughness is defined by the following expression

$$f(x) = \begin{cases} 0, & x < -\frac{d}{2}, \\ \pm \frac{h}{2} (1 + \cos(\frac{2\pi x}{d})), & x \in [-\frac{d}{2}, \frac{d}{2}], \\ 0, & x > \frac{d}{2}, \end{cases} \quad (18)$$

where  $d$  is the streamwise width scale and  $h$  is the normal direction length scale ( $+h$  and  $-h$  denote the height scales of humps and indentations, respectively). The schematic figure of the computational domain is illustrated for hump cases in figure 2(a). In figure 2(b), the elements of the background coarse mesh around the hump are shown. Because we consider that the spectral/ $hp$  element approximation with an element is a polynomial of order  $P$  (eight modes), in order to establish a consistent approximation of the hump geometry boundary, the boundary of the hump is approximated by curved elements with  $P$ -order polynomial expansions of curved edges. In figure 2(c), the high-order mesh with collocation points is shown around the hump. The configurations of the current mesh and the polynomial order were set up based on the  $P$ -refinement independence.

### 3.2 Perturbations of solving LNSEs

In computations, the LNSEs are solved in sub-domains of the original domains in which base flows are generated. In the sub-domains, only the

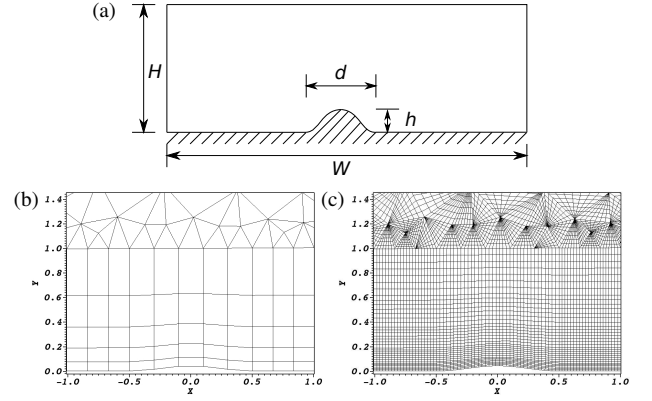


**Fig. 2** Schematic figures of the computational domain and the mesh around a hump: (a) the computational domain with a smooth hump on the lower boundary.  $h$  and  $d$  denote height and width of the hump, respectively; (b) low-order background mesh around the hump; (c) high-order body fitted mesh around the hump.

inlet positions are changed to guarantee that the inlet displacement Reynolds numbers are in the unstable regime of the neutral stability diagram. So, when the inlet displacement Reynolds number  $Re_\delta$  lies in the unstable regime for a given real frequency  $\omega$ , the boundary condition normal component of (6) is defined by the most unstable eigenfunction of the discrete spectrum. Mathematically, the inlet boundary condition is formulated as follows

$$\tilde{u} = \varepsilon \Re[(u_{TS}, v_{TS}) \cdot \exp(-i\omega t)], \quad (19)$$

where  $\varepsilon$  can be arbitrary non-zero constant.  $v_{TS}$  is the most unstable eigenfunction corresponding to the frequency  $\omega$  and  $u_{TS}$  is obtained directly by the divergence-free condition. In simulations, the dimensionless frequency  $\mathcal{F}$  is defined by

$$\mathcal{F} = \frac{\omega}{Re} \times 10^6. \quad (20)$$

## 4 Results

The behaviours of transmitted T-S waves are determined by localized distorted base flows which induce the local change of the boundary layer instability. Typically, shear stress distributions of base flows around small localized imperfection on the wall have a significant contribution to figure out the behaviours of transmitted T-S waves.

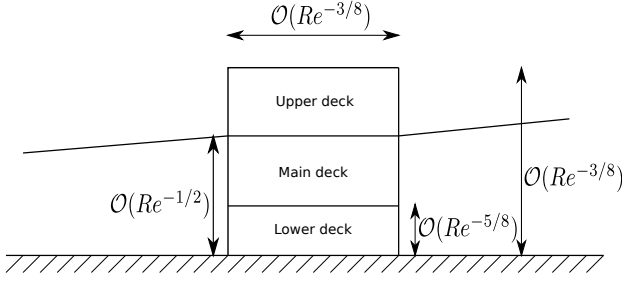


**Fig. 3** Schematic figure of triple-deck structure.

Classically, the triple-deck theory is used to describe and formulate locally distorted base flows (see figure 3 for schematic triple-deck structure). In this section, we firstly review the lower-deck structure and the corresponding linearised approximation. Then, we discuss the shear stress distribution in terms of the linearised lower-deck theory. Finally, we will discuss the availability of the linearised theory for formulating the transmission coefficient. The transmission behaviours are addressed numerically for various configurations.

#### 4.1 Linearised lower deck

Let's recall the classical triple-deck structure [15, 17] and introduce a small parameter  $\varepsilon$ , the asymptotic dimensionless thickness of the oncoming boundary layer, which is defined by

$$\varepsilon = Re^{-1/2}. \quad (21)$$

For the lower deck, the following variables are used

$$X := \lambda^{5/4}x, Y := \lambda^{3/4}y, \quad (22)$$

We denote by  $U_B(Y)$  the non-perturbed Blasius velocity profile of the boundary layer at  $x = x_c$  and its slope at wall,  $\lambda$ , is defined by

$$\lambda = \left( \frac{U_0(Y)}{dY} \right)_{Y=0}, \quad (23)$$

where  $Y = \varepsilon^{-1}y$  is a main deck variable. It is assumed that locally, the hump/indentation has the following profile [15]

$$y/x_c = \varepsilon^{5/4} \hat{h} F(X), \quad (24)$$

where  $\hat{h}$  is initially of the order one and the function  $F$  is such that  $\hat{h}F(X)$  is of the order one or

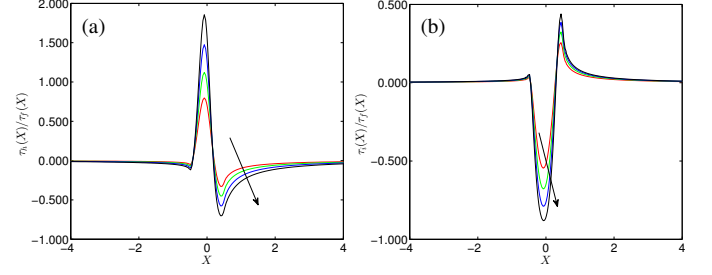


**Fig. 4** Shear stress distributions around small-scale humps and indentations: (a) shear stress distributions around humps; (b) shear stress distributions around indentations.  $Re_{\delta_*} = 1140.1$ . Height/depth  $\hat{h} = 0.6, 0.8, 1, 1.2$  and width  $\hat{d} = 1$ .

less. Consider now  $\bar{h} \ll 1$  ( $\bar{h}$  is a redefined scale of  $\hat{h}$  in terms of the scale along the  $y$ -direction in (22)), in terms of the arguments of subsonic flows [15], the following approximate relations hold for the linearised lower deck equations

$$\frac{d\hat{p}}{dX} = \frac{\bar{h}\theta^3}{2\pi} \int_{-\infty}^{\infty} F(X-t)\alpha(t)dt, \quad (25a)$$

$$\tau = 1 - \frac{3\bar{h}Ai(0)\theta^{4/3}}{2\pi} \int_{-\infty}^{\infty} F(X-t)\beta(t)dt, \quad (25b)$$

where  $Ai(X)$  denotes Airy function and  $\theta = [-3Ai'(0)]^{3/4}$ .  $\alpha(t)$  and  $\beta(t)$  are two special functions of  $t$  (see [15] for more details). For the fixed shape  $F(X)$ , (25) and (25) are independent of the integrals at the right hand sides of (25). Therefore, the following scaling relations hold

$$\frac{d\hat{p}}{dX} \sim \hat{h}, \tau \sim 1 + \hat{h}. \quad (26)$$

Changing the sign in front of  $\hat{h}$ , the above relations also hold for indentation.

#### 4.2 Shear stress and pressure distributions

To investigate the influence of hump/indentation on behaviours of transmitted T-S waves and assess the availability of  $\mathcal{T}_{h,i}(\infty)$  estimation by the linearised lower-deck theory, shear stress and pressure distributions are calculated around roughness positions. Figure 4 shows the normalized shear stress distributions with respect to different values of  $\hat{h}$  for humps and indentations. From here on, arrows in figures indicate the growth direction of height/depth scales except for

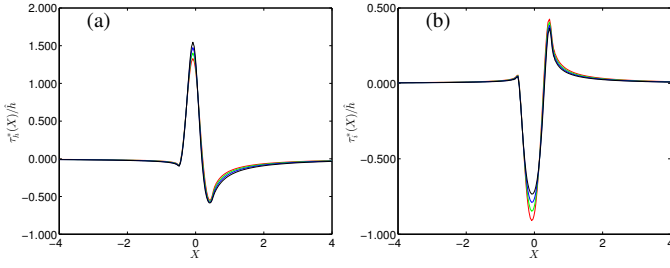


**Fig. 5** Shear stress distribution normalized by  $\hat{h}$  around small-scale humps and indentations: (a) normalized shear stress distribution around humps; (b) normalized shear stress distribution around indentations.  $Re_{\delta_*} = 1140.1$ . Height/depth  $\hat{h} = 0.6, 0.8, 1, 1.2$  and width  $\hat{d} = 1$ .

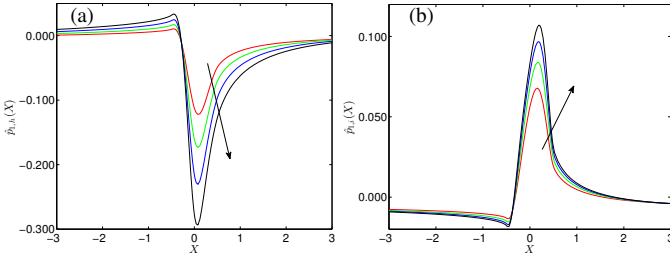


**Fig. 6** Pressure distribution around small-scale humps and indentations: (a) pressure distribution around humps; (b) pressure distribution around indentations.  $Re_{\delta_*} = 1140.1$ . Height/depth  $\hat{h} = 0.6, 0.8, 1, 1.2$  and width  $\hat{d} = 1$ .

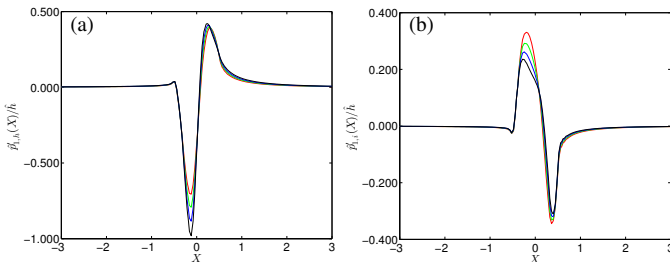


**Fig. 7**  $dP(X)/dX$  distribution normalized by  $\hat{h}$  around small-scale humps and indentations: (a) normalized  $dP(X)/dX$  distribution around humps; (b) normalized  $dP(x)/dX$  distribution around indentations.  $Re_{\delta_*} = 1140.1$ . Height/depth  $\hat{h} = 0.6, 0.8, 1, 1.2$  and width  $\hat{d} = 1$ .

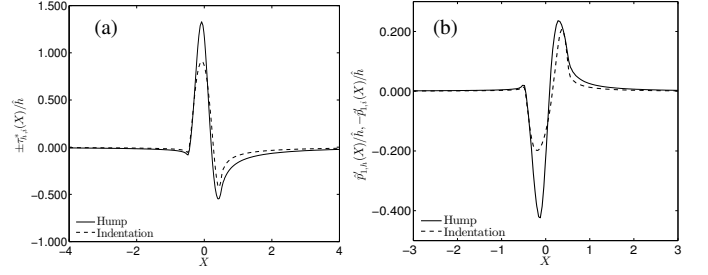


**Fig. 8** Shear stress and  $dP(X)/dX$  distributions normalized by  $\hat{h}$  around small-scale humps and indentations: (a) normalized shear stress distributions; (b) normalized  $dP(X)/dX$  distributions.  $Re_{\delta_*} = 1140.1$ . Height/depth  $\hat{h} = 0.6$  and width  $\hat{d} = 1$ .

special remarks. In terms of (26), the following relations hold

$$\tau_h^*(X) \sim \hat{h}, \tau_i^*(X) \sim \hat{h}. \quad (27)$$

Then, the normalized  $\tau_h^*(X)$  and  $\tau_i^*(X)$  by  $\hat{h}$  should collapse, which are illustrated in figure 5. It is clear that the different curves collapse partially. However, around maximum/minimum values of (27), the deviations among the normalized quantities are observed. For the current small parameters, the obtained results do not support the linearised lower-deck prediction very well. Figure (6) shows the pressure distributions  $\hat{p}_{1,h}(X)$  and  $\hat{p}_{1,i}(X)$  around humps and indentations. Considering (26), the normalized  $d\hat{p}_{1,h}(X)/dX$  and  $d\hat{p}_{1,i}(X)/dX$  by  $\hat{h}$  also should collapse. From figure (7), it is observed that although the curves collapse, there still exist some significant deviations from theoretical prediction. Moreover, figure 8 shows comparisons between a hump and an indentation for the same  $\hat{h}$ . According to the linearised lower-deck theory, with small  $\hat{h}$  value,  $\tau_h^*(X)/\hat{h}$  and  $-\tau_i^*(X)/\hat{h}$  should have the same profile and meanwhile, the same argument should also be held for  $d\hat{p}_{1,h}(X)/dX$  and  $-d\hat{p}_{1,i}(X)/dX$ . But, we do not get the coincident conclusion with the theoretical prediction from figure 8. For small humps/indentations, there exists a significant deviation of the above mentioned numerical results from the linearised theoretical results. That means for the fixed  $\hat{h}$ , the accuracy of the linearised theory is significantly dependent on  $\hat{d}$ . That is to say, although  $\hat{h}$  is very small, the prediction precision is strongly dependent on the

value of  $\hat{h}/\hat{d}$ .

### 4.3 Behaviours of transmitted T-S waves

To formulate the influence of hump and indentation on T-S waves, the transmission coefficient is introduced to quantify T-S wave behaviours [1]. As illustrated in figure 9, the theoretical definition of the transmission coefficient and the analytical expression to leading order were introduced by [1]

$$\mathcal{T}_r = A_T^{\max}/A_I^{\max}, \quad (28a)$$

$$\mathcal{T}_r = 1 + C\varepsilon^{\frac{1}{4}}\hat{h}\hat{F}(0), \quad (28b)$$

where  $\hat{F}(k - \alpha)$  is Fourier transform of roughness element and  $C$  is a constant dependent on  $\alpha, \alpha_1, \alpha_2$  and  $\eta_0$  (see [1] for details). In the formulation, the T-S wave has a wavenumber  $\alpha$  and the mean-flow distortion has a continuous Fourier spectrum, which is a continuous function of wavenumber  $k$ . It was predicted that (28) indicates that roughness shape is irrelevant, and the gain or reduction in the T-S wave amplitude is proportional to  $S \equiv \hat{h}\hat{F}(0)$ , which is the (rescaled) area enclosed by the roughness contour.

As indicated by (28), the hump can stabilize T-S waves and the indentation can destabilize T-S waves. Figures 10 and 11 show that the behaviours of transmitted T-S waves. Within a small range of  $X \in [-6, 6]$ , it may be possible that T-S waves can be stabilized ( $\mathcal{T}_h(X) < 1$ ) downstream by small-height hump in figure 10(a). But, this is not true. Figure 10(b) shows that the stabilized T-S wave is destabilized further downstream again. For the current configurations, it is concluded that humps and indentations have the similar destabilization influence on T-S waves. It is also observed that with the same  $\hat{h}$ ,  $\mathcal{T}_h(\infty)$  is greater than  $\mathcal{T}_i(\infty)$  ( $X \gg 1$ ).

Further, theoretical result of (28) indicated that  $\mathcal{T}_r$  is only dependent on  $\hat{h}$  for the fixed roughness profile  $F(X)$ . That is to say,  $\mathcal{T}_h^*(X)/\hat{h}$  and  $\mathcal{T}_i^*(X)/\hat{h}$  should collapse around humps and indentations. But, figures 12 and 13 show that the approximate collapse phenomena only occur within a small range  $X \in [-1, 1]$ . Beyond this range, the distorted T-S waves do not hold the

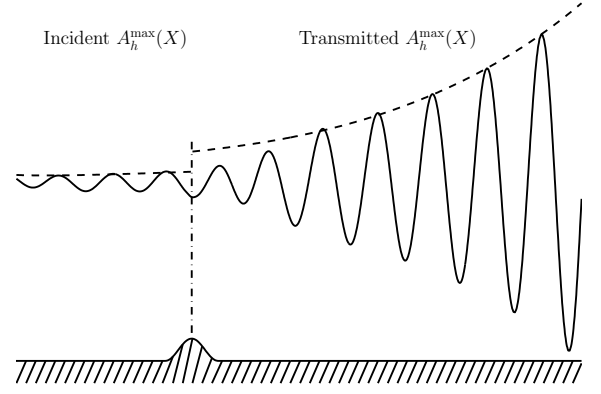


**Fig. 9** Schematic illustration of transmitted T-S waves distorted by a hump.

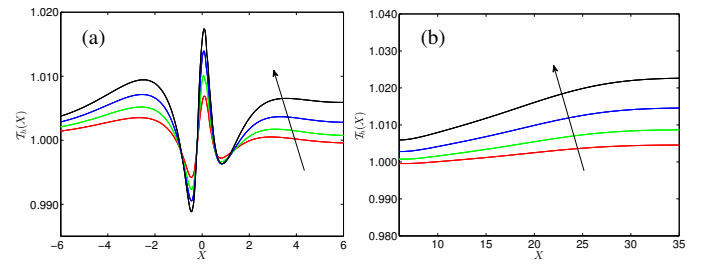


**Fig. 10**  $\mathcal{T}_h(X)$  around humps: (a)  $\mathcal{T}_h(X)$  for  $X \in [-6, 6]$ ; (b)  $\mathcal{T}_h(X)$  for further down stream.  $Re_{\delta_*} = 1140.1$  and  $\mathcal{F} = 55.10$ .  $\hat{h} = 0.6, 0.8, 1, 1.2$  and width  $\hat{d} = 1$ .

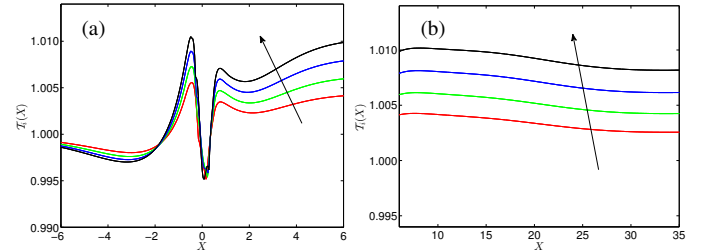


**Fig. 11**  $\mathcal{T}_i(X)$  around indentations: (a)  $\mathcal{T}_i(X)$  for  $X \in [-6, 6]$ ; (b)  $\mathcal{T}_i(X)$  for further down stream.  $Re_{\delta_*} = 1140.1$  and  $\mathcal{F} = 55.10$ .  $\hat{h} = 0.6, 0.8, 1, 1.2$  and width  $\hat{d} = 1$ .

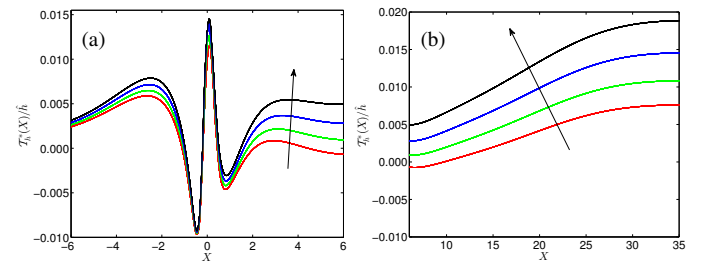


**Fig. 12**  $\mathcal{T}_h^*(X)/\hat{h}$  around humps: (a)  $\mathcal{T}_h^*(X)/\hat{h}$  for  $X \in [-6, 6]$ ; (b)  $\mathcal{T}_h^*(X)/\hat{h}$  for further down stream.  $Re_{\delta_*} = 1140.1$  and  $\mathcal{F} = 55.10$ .  $\hat{h} = 0.6, 0.8, 1, 1.2$  and width  $\hat{d} = 1$ .

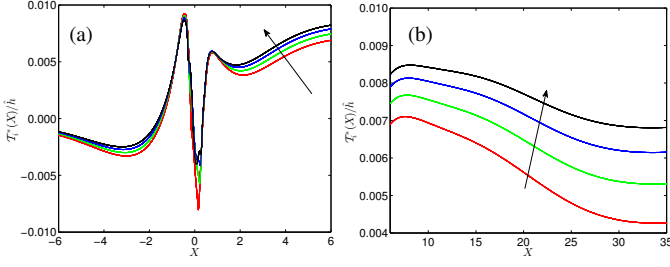


**Fig. 13**  $\mathcal{T}_i^*(X)/\hat{h}$  around indentations: (a)  $\mathcal{T}_i^*(X)/\hat{h}$  for  $X \in [-6, 6]$ ; (b)  $\mathcal{T}_i^*(X)/\hat{h}$  for further down stream.  $Re_{\delta_*} = 1140.1$  and  $\mathcal{F} = 55.10$ .  $\hat{h} = 0.6, 0.8, 1, 1.2$  and width  $\hat{d} = 1$ .

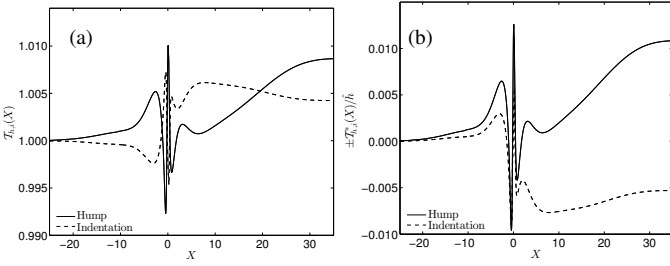


**Fig. 14** Comparisons of  $\mathcal{T}_{h,i}(X)$  and  $\mathcal{T}_i^*(X)/\hat{h}$  around hump and indentation: (a)  $\mathcal{T}_{h,i}(X)$ ; (b)  $\mathcal{T}_i^*(X)/\hat{h}$  and  $-\mathcal{T}_i^*(X)/\hat{h}$ .  $Re_{\delta_*} = 1140.1$  and  $\mathcal{F} = 55.10$ .  $\hat{h} = 1$  and width  $\hat{d} = 1$ .

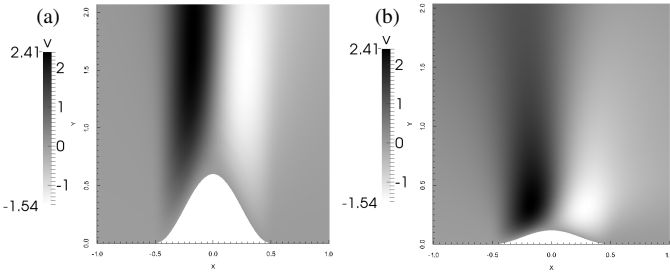


**Fig. 15** Vertical velocity fields: (a) vertical velocity is rescaled by  $\varepsilon$  and  $y$  rescaled by  $\varepsilon^{5/4}$ ; (b) vertical velocity is rescaled by  $\varepsilon$  and  $y$  rescaled by boundary layer scale.  $Re_{\delta_*} = 1140.1$ .  $\hat{h} = 0.6$  and width  $\hat{d} = 1$ .

theoretical scaling relation. Clearly, thanks to the distortion, the boundary layer instability is changed and locally, the T-S waves do not hold the similar growth and decay rates to those of the T-S waves in the Blasius boundary layer. [1] argued that the effect of a localized roughness element is to ‘boost’ instantly the amplitude of the T-S wave amplitude. But, the numerical evidence shows that the argument is inapplicable. In figure 14, a comparison for a hump and an indentation with the same value of  $\hat{h}$  is given. From 14(a), it is clearly observed that when  $X \rightarrow \infty$ , the influence of humps on T-S waves is more than that of indentations. From 14(b), the sign in (28) indicates the different downstream behaviours of T-S waves but not the similar behaviours. In figure 15, the rescaled vertical velocity of a base flow around a hump is illustrated locally. Around the hump, the freestream vertical velocity scale can be observed. It indicates that thanks to the subsonic ellipticity property, momentum is redistributed and the approximate Blasius boundary layer does not exist locally. By the nonlinear mechanism, the flow structure past a hump is completely different from the flow structure generated by the linear extrapolation. For the current cases, the trivial Taylor expansion can not be used to establish an approximate relation between the flow generated by the linear extrapolation and the flow generated by the nonlinear mechanism, although the  $\hat{h}$  is small. Therefore, we can say that the T-S wave transmission behaviours can not be described by a linearised theory under the current parameter configurations.

## 5 Further discussion and conclusion

In this paper, the high precision spectral element method is employed to implement the computations and analyse the behaviours of the T-S waves when the base flows are distorted by small-scale localized roughness. From numerical point of view, the present approach, which achieves high-precision high-fidelity results by using high-order polynomials, has a certain reliability for addressing local roughness problems on boundary layers in detail. The base flows are generated by fully non-linear simulations and the T-S waves are

simulated by the linearised Navier-Stokes equations. The related analysis is quite important to understand the real physics of the transmitted T-S waves.

We demonstrated that the numerical evidences are against the arguments of the energizing or weakening of T-S waves by the interaction with localized roughness elements. According to the asymptotic analysis, the analytical definition (28) of transmission coefficient is defective, at least for subsonic flows. From the results, we conclude that with very small  $\hat{h}$ , there exists a region where  $\mathcal{T}_h(X)$  is small than 1. However, as indicated by numerical results, the weakening of the T-S waves by humps is a local property. This phenomenon does not disclose the real physics for further downstream. After decaying within a small range, the T-S waves grow again and the growth rate goes back to that of the flat plate boundary layers when the flat plate boundary layer profiles recover. Then,  $\mathcal{T}_h(X)$  is constant. For indentations, although the amplitudes of the T-S waves are much energized behind indentions,  $\mathcal{T}_i(X)$  decays and intends to be constant when  $X \gg 1$ . For humps and indentations, when the flat plate boundary layer recovers,  $\mathcal{T}_i(\infty) < \mathcal{T}_h(\infty)$ . As indicated by figure 9, on two sides of the vertical dash-dot line, the amplitude of the T-S wave at the centre position of the roughness element has a jump if on both sides there exist two exact flat plate boundary layers. Because on both sides, there are no flat plate boundary layers, the calculating of  $\mathcal{T}(\infty)$  by the extrapolation of the T-S amplitudes from both sides of roughness will give rise to inaccurate results, even wrong results. Practically, a reference T-S wave amplitude  $A^{\max}(X)$  is needed for calculating  $\mathcal{T}(\infty)$ . If the roughness elements are placed close to upper branch, the calculation of transmission coefficient  $\mathcal{T}(\infty)$  is useless, thanks to the requirement of the long downstream distance along which the T-S waves decay.

The present study further indicates that a minimal localized hump has a worse effect on the T-S waves compared with a minimal localized indentation if the hump and the indentation are close to lower branch.

## 6 Acknowledgements

The authors would like to thank Prof. X.S. Wu for the useful discussion. This research was performed in the Laminar Flow Control Centre (LFC-UK) at Imperial College London. The Centre is supported by EPSRC, Airbus UK and EADS Innovation Works.

## References

- [1] Wu X. S. and Hogg L. W. Acoustic radiation of tollmien schlichting waves as they undergo rapid distortion. *J. Fluid Mech.* Vol. 550, pp 307-347, 2006.
- [2] Schlichting H. and Gersten K. *Boundary-Layer Theory.* Mac Graw-Hill, 1968.
- [3] Schubauer G. B. and Skramstad. H. K. Laminar-boundary-layer oscillations and transition on a flat plat. NASA TR-909, 1948.
- [4] Schmid P. J. *Stability and transition in shear flow.* Springer-Verlag New York, 2001.
- [5] Gaster M. On the generation of spatially growing waves in a boundary layer. *J. Fluid Mech.* Vol. 22, pp 433-441, 1965.
- [6] Murdock J. W. The generation f a Tollmien-Schlichting wave by a sound wave. *Proc. R. Soc. Lond. A.* Vol. 372, pp 571-534, 1980.
- [7] Goldstein M. E. 1983 The evolution of Tollmien-Schlichting waves near a leading edge. *J. Fluid Mech.* Vol. 127, pp 59-81, 1983.
- [8] Kerschen E. J. Boundary layer receptivity theory. *Appl. Mech. Rev.* Vol. 43, pp S152-S157, 1990.
- [9] Dietz A. J. Local boundary-layer receptivity to a convected free-stream disturbance. *J. Fluid Mech.* Vol. 378, pp 291-317, 1999.
- [10] Wu X. S. Receptivity of boundary layers with distributed roughness to vortical and acoustic disturbances: a second-order asymptotic theory and comparison with experiments. *J. Fluid Mech.* Vol. 431, pp 91-133, 2001.
- [11] Saric W. S., Reed H. L. and Kerschen E. J. Boundary-layer receptivity to free-stream disturbances. *Annu. Rev. Fluid Mech.* 34, 251-276, 2002.
- [12] Smith J, Jones B and Brown J. The title of the journal paper. *Journal Name,* Vol. 1, No. 1, pp 1-11, 2001.

- [13] Corke T. C., Sever A. Bar and Morkovin, M. V. Experiments on transition enhancements by distributed roughness. *Phys. Fluids* Vol. 29, pp 3199-3213, 1986.
- [14] Wörner A., Rist U. and Wagner S. Humps/steps influence on stability characteristics of two-dimensional laminar boundary layer. *AIAA*. Vol. 41, No. 2, 192-197, 2003.
- [15] Smith, F. T. Laminar flow over a small hump on a flat plate. *J. Fluid Mech.* Vol. 57, pp 803-824, 1973.
- [16] Karniadakis G. E. and Sherwin S. J. *Spectral/hp Element for Computational Fluid Dynamics*. Springer-Verlag New York, 2005
- [17] Cousteix J. and Mauss J. *Asymptotic Analysis and Boundary Layers*. Springer-Verlag Berlin Heidelberg. 2007.

### Contact Author Email Address

mailto: hui.xu@imperial.ac.uk

### Copyright Statement

The authors confirm that they, and/or their company or organization, hold copyright on all of the original material included in this paper. The authors also confirm that they have obtained permission, from the copyright holder of any third party material included in this paper, to publish it as part of their paper. The authors confirm that they give permission, or have obtained permission from the copyright holder of this paper, for the publication and distribution of this paper as part of the ICAS 2014 proceedings or as individual off-prints from the proceedings.